Integration of an Optical Electric Field Sensor in Lithium Niobate on Insulator

Journal Article

Author(s):
Wackernagel, Daniel (ID); Kaufmann, Fabian; Maeder, Andreas; Grange, Rachel (ID); Franck, Christian M.

RESEARCH ARTICLE

Integration of an Optical Electric Field Sensor in Lithium Niobate on Insulator

DANIEL WACKERNAGEL[1], **FABIAN KAUFMANN**[2], **ANDREAS MAEDER**[2], **RACHEL GRANGE**[2], **AND CHRISTIAN M. FRANCK**[1], (Senior Member, IEEE)

[1]High Voltage Laboratory, Institute for Power Systems and High Voltage Technology, Department of Information Technology and Electrical Engineering, Swiss Federal Institute of Technology (ETH) Zürich, 8092 Zürich, Switzerland
[2]Optical Nanomaterial Group, Institute for Quantum Electronics, Department of Physics, Swiss Federal Institute of Technology (ETH) Zürich, 8093 Zürich, Switzerland

Corresponding author: Daniel Wackernagel (daniewac@ethz.ch)

ABSTRACT Sensors are a major component in any experimental set-up. In a high voltage environment, the aspect of safety must be particularly emphasized and the galvanic isolation is often provided by an optical communication link in between the "electric-sensor" and the "detection-unit". However, the transformation of electrical to optical signals and back can introduce delays and errors. To mitigate this, electric fields were directly measured with an in-house fabricated optical sensor chip, based on lithium niobate. On the one hand we measured locally with electrodes on chip, on the other hand in an external electric field across the sensor. Here, we measured a sensitivity of $\sim$(8 mV)/(10 kV/cm) on the chip with peak ac field strengths up to 11 kV/cm and $\sim$(10 mV)/(1 kV/cm) in free space for 2 kV/cm at net frequency of 50 Hz. Hysteresis effects on the sensor were found to be decreased for the free space arrangement. Thus, the fabrication and test procedures work effectively and the electric field measurements showed a good agreement of the performance comparing the on-chip and free space set up. This allows for fast and easy on-chip testing of new resonator based sensors to optimize the geometry and adapt the sensor to its application.

I. INTRODUCTION TO HIGH VOLTAGE MEASUREMENT TECHNIQUES

In the area of high voltage engineering, there are different devices and procedures that are commonly used to measure high voltages. When measuring high voltages, one needs to convert the high voltage into a smaller signal which can be measured with standard methods, such as an oscilloscope. This is done using dividers which each have their advantages and drawbacks.

Different classical resistive and capacitive dividers are used for various measurements and are typically optimised for a specific frequency range [1]. All of them share the disadvantage of having a direct and galvanic connection between the high voltage potential and the measurement device. This

The associate editor coordinating the review of this manuscript and approving it for publication was Andrea De Marcellis .

cannot only be dangerous for the oscilloscope and for the people working nearby, but is also prone to couple electromagnetic noise.

To increase safety and avoid a galvanic connection, two methods are applied. The indirect principle is to measure the signal classically, but placing the measurement device inside the high voltage circuit and only transmitting the measurement data optically or wireless [2]. The other possibility is to use measurement devices directly based on optical principles [3]. This means that the measurement device is not electrically connected to the high voltage circuit, thus enabling a safe operation of the experiment and also reduces additional noise introduction.

One possibility of constructing such an optical measurement device is to use electro-optical effects in bulk crystals for voltage measurements [3], potential distribution [4] or integrated on chip [5] to modulate an optical

laser signal, similar to how electrical signals are encoded in long and short haul telecommunication systems [6]. The electro-optical effect (Pockels effect) used in these applications changes the refractive index of the crystal. It can be used to alter the phase of the light or to modulate the amplitude where additional interferometer structures are needed. The same effect is used with Mach-Zehnder modulators to modulate an optical laser signal, similar to how electrical signals are encoded in long and short haul telecommunication systems.

The idea is to construct an integrated device, but instead of using the extreme digital on-off signal, the whole signal range in between those levels will be measured, in order to relate the output laser intensity to the applied electrical field. Ideally this can be realized in a small device and the chosen material would offer a wide range of frequency applications. A small device would not only be favorable due to small mechanical size (less than 1 cm^2) but would also be less sensitive to electromagnetic interference and distort the external field less. The material lithium niobate (LN) is chosen as it is often used in optical communication and the availability of the in-house fabrication for thin film chips is given. Research in the optical community focuses mainly on the high frequency range and strives to enable the next generation of optical communication by increasing the bandwidth beyond 67 GHz [7], [8], [9]. For the electric field measurement in high voltage engineering, sensors in a different frequency range are required.

The main aim of this contribution is to demonstrate that it is possible to measure electric field strengths with an integrated optical sensor manufactured from a thin film lithium niobate chip without local electrodes. For this, a systematic approach including all steps of development is followed and presented in the respective sections of this paper. To confirm the suitability of the LN material, a commercially available Mach-Zehnder modulator (MZM) for optical data-transmission is characterised in section II. The focus lies thereby on the aptitude for typical electrical frequencies (Hz to several MHz). To validate the suitability of the in-house fabrication, the test procedure (i.e. how to connect the chip optically and electrically) and the adaptation of the structure to Lithium Niobate on insulator (LNOI), a self-fabricated MZM was characterised first (section III). To continue in section IV, an on-chip ring resonator is fabricated and tested with electric fields applied locally with electrodes on the chip, similar to [7]. Due to the steep flank of the resonance, a small change in phase introduces the desired amplitude modulation by applying an external varying electric field. In the last step, section V, the ability to measure high voltage fields in free space is investigated. The electrical and optical circuit (including a custom 3D printed fiber alignment stage [10], [11]) are introduced and used for the test with the on-chip resonator. The chip is prepared by taking off the electrodes and afterwards characterised in the free space high voltage setup.

II. LOW FREQUENCY RESPONSE OF LITHIUM NIOBATE MATERIAL
The main application of electro-optical modulators today is for high-speed optical telecommunication with fiber [6] and operate at up to 40 GHz. For the application in high voltage measurement instruments, the required frequency range is from dc to a few tens of MHz, for which the material properties are also known, but dc drift is a big issue that has to be overcome [12]. Since active feedback is not an option for this sensor, in a first step, the suitability to exploit the Pockels effect of lithium niobate (LN) material at lower frequencies is investigated.

A. METHODS
For this, a commercially available Mach-Zehnder Modulator (MZM) is used: a ThorLabs LN81S-FC 10 GHz broadband intensity modulator [13] with an x-cut LN crystal. It's specified operating range is dc to 15 GHz, but the shown measurements are not resolved in the range of interest below 1 GHz. The principle test setup is shown in Fig. 1. The laser [14] is operated at a wavelength of 1550 nm and its light is guided with a polarisation maintaining fiber (PMF) to the MZM. After the modulator, the optical signal is guided to a 5 GHz InGaAs photo detector (PD) DET08CFC/M [15] with a single mode fiber (SMF). An electrical modulation signal is generated by a Bode 100 [16] vector network analyzer (VNA), which is connected to the RF-input of the modulator with a coaxial cable, using a BNC-to-SMA adapter. The operating range of the VNA is 1 Hz to 50 MHz. The PD output signal is connected back to the VNA. To set the working point, a dc power supply [17] is connected to designated dc bias input. The output signal of the internal PD is not used in this measurement and is left open.

By applying an ac modulation voltage to the MZM the dc bias is set to be at the quadrature point. The VNA measures the forward transmission $\mathcal{T}$, which is defined as $\mathcal{T} = V_{in}/V_{out}$ and expressed in decibel with V_{in} being the measured voltage of the PD at the input of the VNA and V_{out} the applied voltage to the MZM from the output of the VNA. For the measurement, the VNA power was set to -10 dBm which yields an output voltage range from $V_{out} = -1$ to $+1$ V. Given the half wave-voltage of $V_\pi = 5.6$ V at $f = 1$ GHz this ensures staying in the linear area around the working point of the MZM.

B. RESULTS AND DISCUSSION
The results obtained from this measurement are shown in Fig. 2. It can be seen that the forward transmission $\mathcal{T}$ is constant within 2 dB over the full frequency range from 1 Hz to 50 MHz. The signal-to-noise ratio is high enough to resolve a fine structure: $\mathcal{T}$ is constant within ± 0.1 dB from 1 Hz to 10 kHz with one disturbance at 50 Hz. From 10 to 2000 kHz, the transmission drops with ~ 0.4 dB per decade. In the range of 2 to 50 MHz, the signal is again constant, but fluctuates with ± 0.5 dB. A -1.3 dB interference can be seen at 50 Hz,
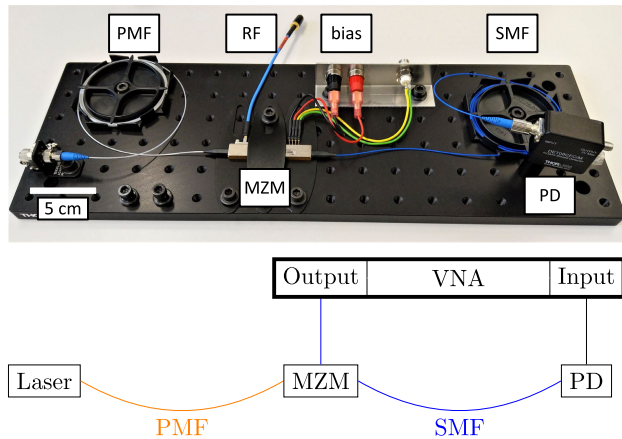
FIGURE 1. Photo and schematic of the measurement setup using a commercial Mach-Zehnder Modulator (MZM). The polarization maintaining fiber (PMF) is shown in orange and the single mode fiber (SMF) in blue. An external photodiode (PD) is used to measure the modulated laser intensity. The electrical signals are generated and measured by a vector network analyzer (VNA). For clarity, the connectors to the used dc bias (black and red) and the not used internal detector (yellow and green) are not included in the schematic.
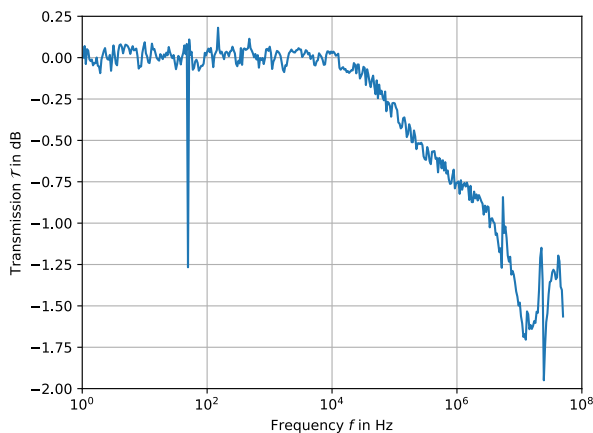

FIGURE 2. The forward power transmission $\mathcal{T}$ is plotted as a function of the electrical frequency f. Plotted in blue is the measured signal using the setup seen in Fig. 1 with the commercial MZM.

which can be explained by the imperfection of the measurement system to filter out the power frequency. The decreasing slope above $f = 10$ kHz is attributed to multiple causes, e.g. bias point drift, MZM material or electrical configuration.

It can be concluded that the electro-optic response of Lithium Niobate is not only constant in the range of several GHz, as shown in the vendor data sheet, but also in the range from several Hz to MHz. Thus the suitability of LN for an electric field sensor is given and an optical sensor in this frequency range, in particular at 50 Hz can be based on this material.

III. FABRICATION AND CHARACTERIZATION OF LNOI STRUCTURES USING THE EXAMPLE OF THE MACH-ZEHNDER MODULATOR

In the previous section it was shown that LN is a suitable material in the required low-frequency range of this project.
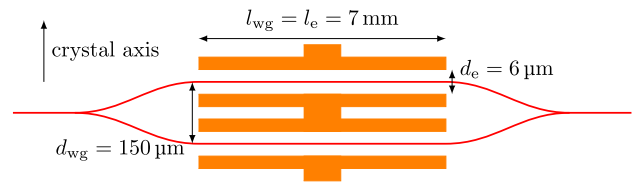

FIGURE 3. Schematic representation of the MZM with its characteristic dimensions. The optical waveguide is drawn in red, the electrodes in orange (distances are not to scale).

The final goal of the project is to establish electrode-free modulators to measure high electric field strengths, using micro-fabricated LN on Insulator (LNOI) chips. The LNOI wafers are bought but the layout can be produced in-house. The used technology features ridge waveguides on the LNOI platform and shows a strong confinement of the optical mode. In this section the LNOI fabrication process is validated and the methods for testing such a chip are defined on the example of a MZM with electrodes.

A. METHODS

A basic MZM layout was chosen for the LNOI chip in this section and is depicted in Fig. 3. The overall length of the MZM is 10 mm with the two MZM arms of length $l_{wg} = 7$ mm and a separation of $d_{wg} = 150$ μm between them. All waveguides have the same width of 600 nm ensuring single mode operation at telecommunication wavelengths. The electrodes are placed symmetrically around the waveguides with length $l_e = 7$ mm and gap distance $d_e = 6$ μm. These dimensions have been chosen to obtain an adequate modulation at the voltage that will be applied later (a few volts). The layout was realised on a x-cut LNOI chip with a 600 nm thin film of LN on an insulating layer (2 μm thermal oxide) on Silicon substrate (0.525 mm) bought from NanoLN. The waveguide fabrication process is divided into the following sub-steps: sample preparation, electron beam lithography, LN dry-etching, mask removal, and wet-etch cleaning of redeposited Lithium Niobate [8]. A SEM image of the waveguide is shown in Fig. 5(a). Electrodes are fabricated using a standard double-layer lift-off process with electron beam evaporation of the metal. Finally, the metal lift-off was performed in a DMSO bath [18].

To compare the performance with the commercial MZM similar measurements were done. The principal setup shown in Fig. 4 is used to test this in-house fabricated MZM. The laser light is guided with a PMF to the MZM chip. There, it is coupled from the lensed fiber-tip to the waveguide on the edge of the chip, see Fig. 5(b). After the modulator, the same coupling technique is used and the optical signal is guided to a 5 GHz InGaAs photo detector (PD) DET08CFC/M [15] with a single mode fiber (SMF). Since the couplings required sub micron alignment precision, both fibers were mounted on piezo-stages.

The electric modulation signal is generated by a Bode 100 [16] VNA. It is connected with a coaxial cable to a pair of
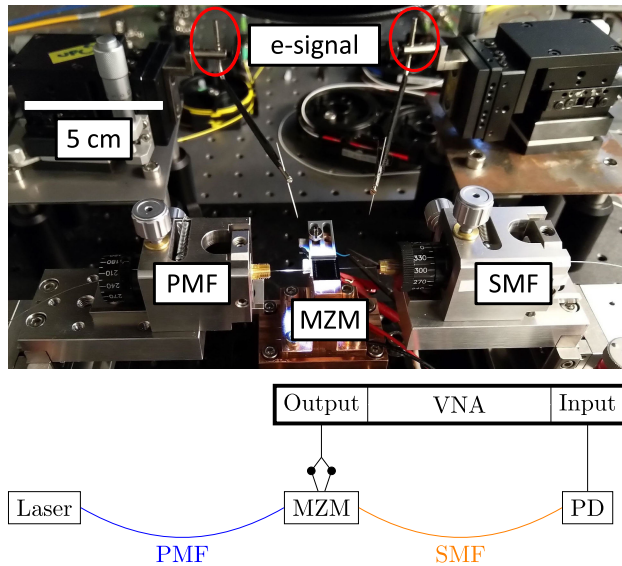
FIGURE 4. Photo and schematic of the measurement setup for the LNOI MZM manufactured in-house. The polarization maintaining fiber (PMF) is shown in blue and the single mode fiber (SMF) in orange. A photodiode (PD) is used to measure the transmitted optical signal. The electrical signals are generated and measured by a vector network analyzer (VNA).
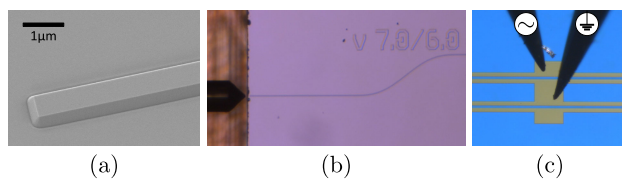

FIGURE 5. SEM and microscopic images of the waveguide, the optical and electrical connections of the MZM chip. (a) The fabricated waveguide with a top width of 600 nm and a height of 300 nm before dicing. (b) Lensed fiber aligned to the waveguide on the chip. (c) Electrodes along the MZM and electrical connection with needle tips.

cables that were soldered to the end of the needle-holder (red circles on top part in Fig. 4). The two needles are then used to electrically contact the device as seen in Fig. 5(c). Hereby, the ground potential was placed in between the two MZM arms and the signal on the side. The PD output signal is connected back to the VNA with a coaxial cable.

By applying a relatively large modulation voltage (> 10 V), the half wave voltage was measured to be $V_\pi \sim 5.9$ V for this MZM. The VNA power was set to -10 dBm which yields an output voltage of $V_{out} = -1$ V to $+1$ V. The tuning of the working point was achieved by tuning the laser wavelength. The forward transmission $\mathcal{T} = V_{in}/V_{out}$ is measured and expressed in decibel for a frequency range $f = 1$ Hz to 50 MHz. All these experiments were performed in a laboratory environment with relatively stable ambient temperature, a study of the temperature dependence of the Pockels effect is not part of this work.

B. RESULTS AND DISCUSSION

The measured power transmission $\mathcal{T}$ is shown in Fig. 6. It can be seen that the transmission $\mathcal{T}$ increases up to $\sim$ 6 dB at
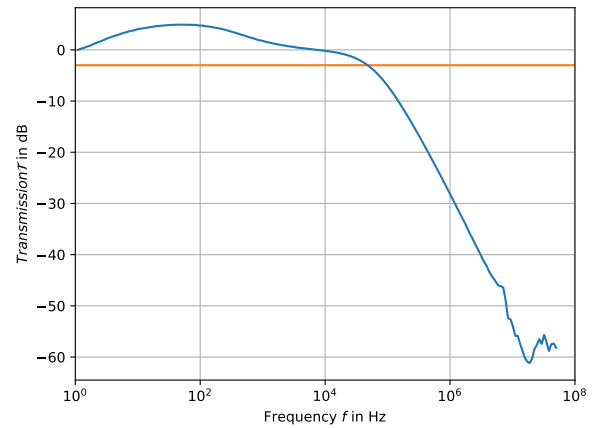

FIGURE 6. The power transmission $\mathcal{T}$ is plotted as a function of the electrical frequency f. Plotted in blue is the measured signal using the setup seen in Fig. 4 with an in-house fabricated MZM. The orange line is shown for reference and indicates the -3 dB threshold.

$\sim$ 80 Hz before decreasing to the initial value of 0 dB at 10 kHz. It remains above the -3 dB threshold up to $\sim$ 80 kHz. For higher frequencies up to 1 MHz the transmission drops with $\sim$ 20 dB per decade before reaching noise floor level of -60 dB.

The overall performance of this simple MZM compares well with the commercial one in the low-frequency range. The strong decrease in signal strength above $\sim$ 80 kHz is caused by the electrical arrangement, namely the lack of RF engineering. The standing wave electrodes on the chip do not achieve the phase matching of the commercial MZM's traveling wave electrodes. This effect is also reinforced by the cables, needles and other surrounding that adds more stray-capacitance compared to the coaxial cables and grounded casing of the commercial MZM and thus more damping for high frequency.

IV. RING RESONATORS WITH ELECTRODES ON CHIP

After the successful fundamental validation of in-house fabricated LNOI-chips using MZM, also ring-resonators (RR) were manufactured. This resonator structure was chosen as it can in principle be operated without electrodes and thus be used to measure electric fields contact-less [19]. In RR, the electro-optical effect leads to a shift in the resonance frequency. With a fixed laser wavelength, an amplitude modulation of the light can be achieved, which can be measured with a photo-diode. In a first step, the RR is tested with electrodes in the same way as the in-house produced MZM.

A. METHODS

The RR is made of two mostly straight waveguides (called bus waveguides) and a ring. It is typically defined by two parameters, the radius r of the ring and the coupling distance c_d (the smallest distance between the bus waveguide and the ring). A schematic, including the electrodes length l_e and distance d_e, is shown on Fig 7. Several different ring resonators, with various parameters, were placed on the same layout as
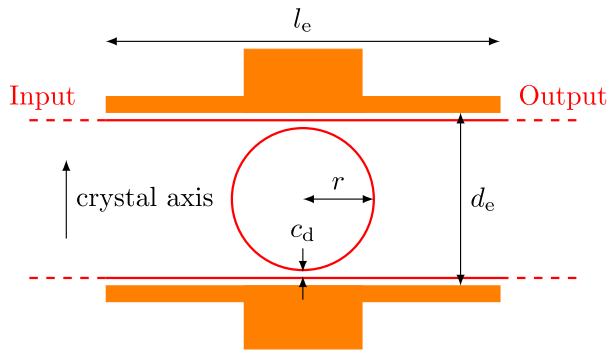
FIGURE 7. Schematic representation of the RR with its characteristic dimensions ring radius r, and coupling distance c_d, together with the electrodes dimensions l_e and d_e. The optical waveguides are drawn in red, the electrodes in orange. The crystal axis of the LNOI is parallel to the chip surface and thus along the e-field. The schematic does not show the full length of the waveguides and is not to scale.

the MZM and thus fabricated with the same procedure as described in Sec. III-A.

Optical and electro-optical measurements were carried out on the ring resonators and are described below. The all-optical measurement aims at determining the optical spectra of the RR. The laser [20] sweeps over a range of wavelengths λ, while the power meter [21] measures the transmitted signal strength on the bus waveguide. A schematic depiction of this is shown in Fig. 8. The laser beam is guided with a PMF to the RR and then with a SMF back to the power meter. The coupling of the optical signal to the chip follows the same steps as described in Sec. III-A.

For the electro-optical test an arbitrary waveform generator (AWG) was used as the voltage source. It was a TiePie [22] that was connected to a high voltage amplifier HVA200 [23] input with a coaxial cable. The HVA output is then connected according to the scheme described in Sect. III-A. For a first measurement the wavelength sweep was repeated with five different applied dc voltages (200, 100, 0, −100, −200 V). Those voltages correspond to field values estimated by $E = V_{out}/d_e = -11.1$ to $+11.1$ kV/cm for $d_e = 180$ nm (radius of ring $r = 80$ μm).

To test the modulation capability, the laser wavelength λ was set to fixed values λ_1 and λ_2. Two points of a resonance dip were chosen to achieve maximum modulation, those were $\lambda_1 = 1549.65$ nm and $\lambda_2 = 1549.91$ nm. The input voltage V_{in} of the RR was measured with the TiePie on the monitor of the HVA. To measure the output voltage V_{out} the power meter was replaced by a photodiode [15] whereby its signal is also recorded with the TiePie. A triangular shaped V_{in} with amplitude of −200 to +200 V and frequency $f = 50$ Hz was applied for both λ_1 and λ_2.

The following results were measured on a ring with radius $r = 80$ μm, coupling distance $c_d = 0.7$ μm and electrode distance $d_e = 180$ μm.

B. RESULTS

The result of the purely optical measurement at the through port of the device is shown in Fig. 9. We see resonance dips of
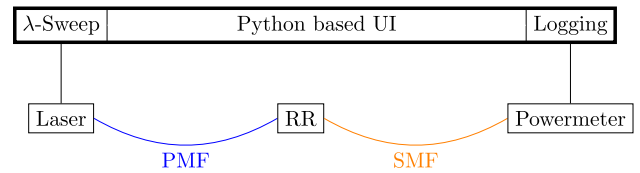

FIGURE 8. Schematic for the measurement setup for the spectrum measurement of the in-house fabricated ring resonators (RR) with electrodes. The polarization maintaining fiber (PMF) is shown in blue and the single mode fiber (SMF) in orange. A power meter is used to measure the transmitted laser power. The laser and power meter are controlled via a Python based user interface.
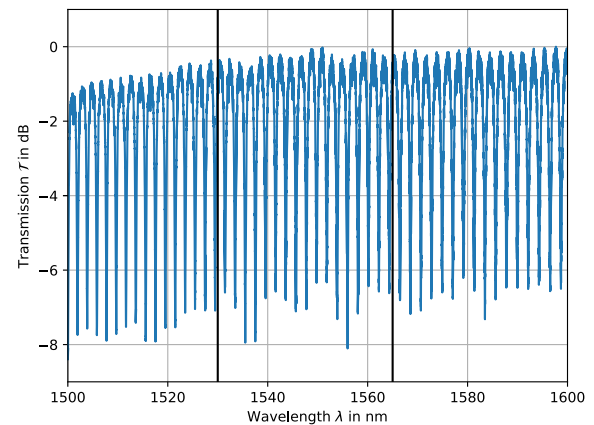

FIGURE 9. The spectrum measurement, i.e. the power transmission $\mathcal{T}$ as a function of optical wavelength λ is plotted for a ring resonator. It is measured according to the setup in Fig. 8. The signal is shifted such that the maximum coincides with 0 dB. The c-band lies between the two black lines.

−6 to −8 dB height that repeat for every $\sim$ 2 nm in the measured laser wavelength range. The maximum values deviate less than 1 dB in the range of the c-band (1530 to 1565 nm). Repeating this measurement yields the same overall shape, up to reduced power throughput due to alignment.

In Fig. 10 we see the detail of one resonance dip in the electro-optical measurement with applied dc voltage. The resonant wavelength shifts in principle symmetrically around the "no field position", for positive fields it shifts towards higher wavelengths. The shift is $\sim$ 55 pm for a field strength of $E = 11.1$ kV/cm. In addition to the resonance, a superimposed oscillation with wavelength $\sim$ 130 pm is clearly visible. It is slightly shifted for each of the measured cases but has a constant amplitude of $\sim$ 0.2 dB. Depending on the relative position of the two effects (RR resonance and superimposed oscillations) the depth and shape of the measured transfer-function varies. On the top left side of the resonance the superimposed oscillation is very regular, on the flanks it seems to skip some oscillations and on the right the signal overall is less smooth.

For the modulation measurement the used wavelengths are indicated by black lines in Fig. 10 and the results are presented in Fig. 11 for a smaller electrical field strength of $\sim$2 kV/cm and in Fig. 12 for a larger range of $\sim$10 kV/cm. The blue and orange curves represent all measurements taken
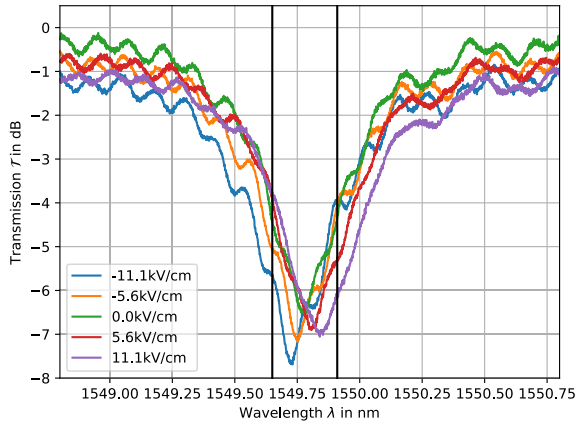
FIGURE 10. Detail of the spectrum measurement, i.e. the power transmission $\mathcal{T}$ as a function of optical wavelength λ, for a ring resonator with applied electrical field is plotted. Different field strengths are indicated by different colors. The black lines indicate the laser wavelengths used in later experiments. The curve without applied electrical field (green) is shifted such that the maximum coincides with 0 dB for easier comparison. All other curves are shifted by the same amount.
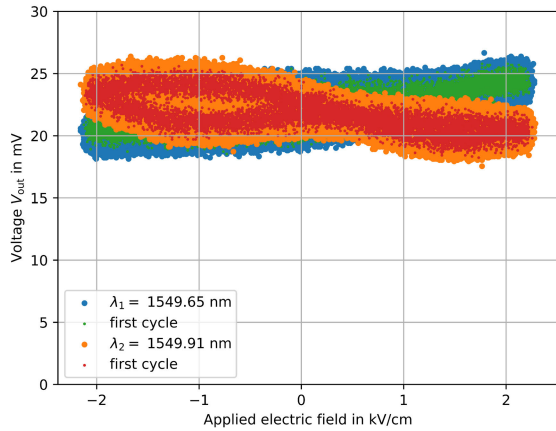

FIGURE 11. Voltage measured with a setup similar to Fig. 4, using the RR instead of the MZM and plotted as a function of the applied electrical field (triangular shape, 50 Hz) for two different wavelengths.

over 50 cycles. The green and red curves represent one example single cycle. While all the measurements show different levels of non-linear behaviour (fluctuating and with hysteresis) a linear relationship between the applied field and the output voltage can be approximated for both λ_1 and λ_2, as well as both field strengths. For λ_1 the slope corresponds to $\sim$(7.5 mV)/(10 kV/cm) and for λ_2 to $\sim$(-8 mV)/(10 kV/cm). This holds true for both field ranges. A hysteresis is visible for both wavelengths and highlighted by the single cycle data (green and red curves). This hysteresis is larger for bigger electric fields. Repeating this measurement can lead to different absolute values caused by the quality of the alignment. In addition the PD would also allow for different amplification settings.

C. DISCUSSION

The spectra of the ring resonator in Fig. 9 shows the expected free spectral range of $\Delta\lambda_{\text{FSR}} = \lambda^2/nL \approx 2.1$ nm with $\lambda =$
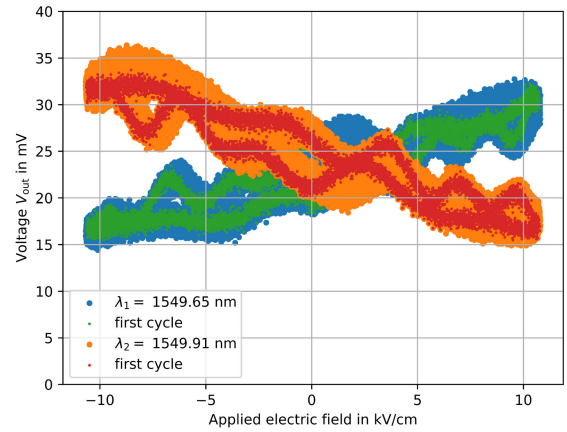

FIGURE 12. Voltage measured with a setup similar to Fig. 4, using the RR instead of the MZM and plotted as a function of the applied electrical field (triangular shape, 50 Hz) for two different wavelengths.

1550 nm, $L = 2\pi \cdot 80\ \mu$m and an estimated refractive index of $n \sim 2.2$ [24] for the LNOI. The height of minimal 6 dB from the resonances corresponds to a power ratio of $\sim$1/4 and an amplitude ratio of $\sim$1/2. This is a good value and will be easily detected in the electro-optical measurements.

The transfer-function of one dip with applied dc voltage across the electrodes in Fig. 10 shows a superimposed oscillation. The free spectral range of $\sim$ 130 pm coincides with $\Delta\lambda_{\text{FSR}} = \lambda^2/nL \approx 135$ pm with $L = 2 \cdot 4$ mm where $\sim$ 4 mm is the total length of the used waveguide. This is therefore a Fabry-Pérot resonance induced by reflections at the two edges of the chip where the light is coupled in and out.

The Pockels effect clearly shifts the resonances in principle symmetrical around the "no-field" point. This allowed two fixed laser wavelengths λ to be chosen (marked with the black lines in Fig. 10) at which a linear relation of the electric field and the laser power can be approximated. The slopes of $\sim$(7.5 mV)/(10 kV/cm) and $\sim$(-8 mV)/(10 kV/cm) indicate that λ_1 and λ_2 were chosen symmetrically around the minima ($|\lambda_1 - \lambda_{\text{min}}| = 123$ pm and $|\lambda_2 - \lambda_{\text{min}}| = 137$ pm) for $\lambda_{\text{min}} = 1549.773$ nm. From Fig. 10 a transmission change of $\sim$ 2 dB is to be expected for $\sim$10 kV/cm and would lead to a measured power ratio of $V_{min}/V_{max} = 1.58$. This is comparable to the measured ratio of $\sim$ 2.

The large noise amplitude and the strong hysteresis however, reduce the accuracy with which this sensor can be used to measure electric fields. The hysteresis is assumed to be caused by charges on the surface of the waveguides and increases for larger electric field amplitudes [25]. The effect of surface charge injection by the electrodes should be eliminated in the following section, where the electrodes are removed and an electrodes free version of the sensor is placed in an external electrical field in free space.

It can be concluded that the RR structure is suitable to detect electrical ac signals and convert them to a measurable laser power modulation.
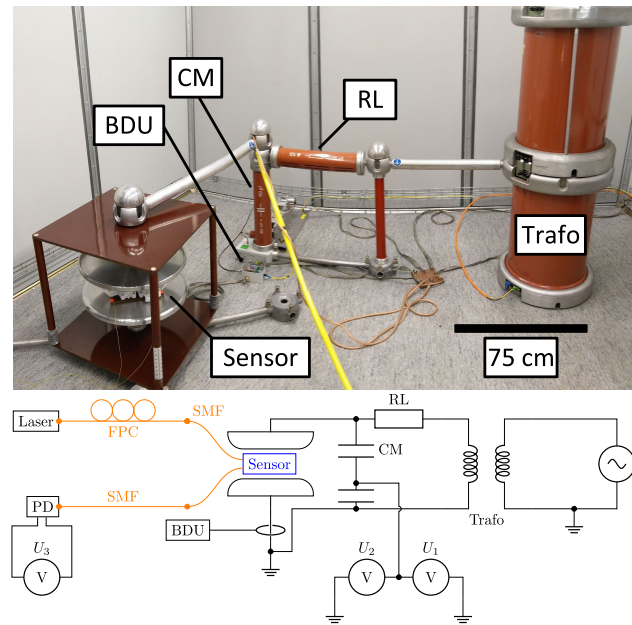
FIGURE 14. Photograph of the 3D printed stage. The chip with the RR is mounted in a vertical and standing position in the middle to have the electric field in the same direction as before with the electrodes on the chip. The distance of the electrode plates is thereby 14 cm and the and the width of the 3D stage in the center measures around 24 cm as indicated in the photograph.

FIGURE 13. Schematic and photograph of the measurement setup for the free space sensor. The laser signal passes the fiber polarization controller (FPC) and afterwards through the sensor. It is then guided back with the single mode fiber (SMF) in orange into a photodiode (PD) which is used to measure the transmitted optical signal as the voltage U_3. The electric field is generated by stepping-up a sinusoidal low-voltage into a high voltage signal by the Trafo. To measure the high voltage, a capacitive divider (CM, 1:1000) reduces the voltage and makes it possible to compare the voltage U_2 to the voltage U_3. U_1 is used as feedback for the PID controller of the voltage generator. For safety, a resistor RL is added to reduce a possible breakdown current. Additionally, a breakdown detection unit (BDU) is used for a quick shutdown of the system.

V. FREE SPACE E-FIELD MEASUREMENT

In the previous section it is shown that a ring resonator is a possible structure to achieve electro-optical amplitude modulation. The measurements were performed locally on chip with gold electrodes. In this section, the sensor is characterised in a free space arrangement.

A. METHODS

The free space experiment consists of the main parts: i) An electrical setup to generate the e-field, ii) the optical parts with the RR sensor and iii) with the laser and photo-diode. A full schematic and a photograph of the electrical setup is depicted in Fig. 13.

A high voltage transformer is connected via a current limiting resistor ($R_L = 50\,k\Omega$) to an electrode gap. It is bounded by two identical flat electrodes with a diameter > 30 cm and an electrode distance of $d = 14$ cm. In addition, a capacitive voltage divider (C_M, 1000:1) is used to measure the applied voltage U_2 and regulate the voltage generator with U_1. For safety, a breakdown detection unit (BDU) is added, which can stop the experiment.

The optical chip was prepared by removing the electrodes in a wet etch process. The optical signal is generated by the c-band laser TLX1 [26] and is guided to the sensor with single mode fibers. To have a defined polarization on the
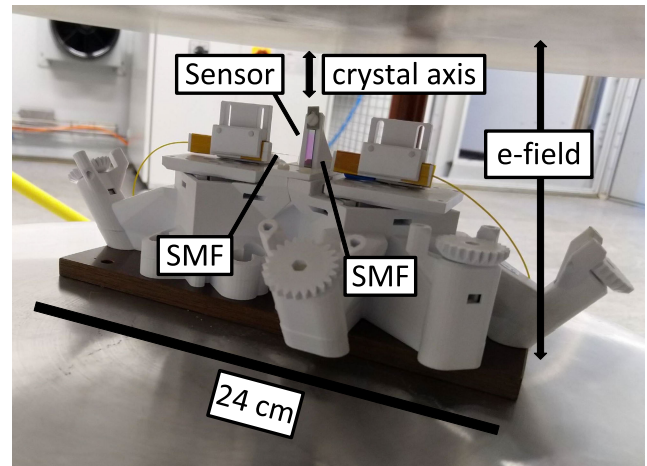
chip, a fiber polarization controller (FPC [27]) was used. After the modulation of the optical signal in the electrode gap, the light is guided to the photo diode [21] with a SMF and U_3 is measured with an oscilloscope. For the alignment of the fiber to the chip, a 3D printed stage [11], [28], made of PLA ($\epsilon_r \sim 3.6$ [29]) was used, see Fig. 14. The chip is thereby in a vertical standing position to achieve the same angle of 90° between the electric field and the normale to the chip's plane (x-axis of LNOI). This stage distorts the e-field only weakly and allows the approximation of the electrical field to be $E = U_2/d$ with $d = 14$ cm. The coupling fibers were stripped and cleaved on the sensor side.

The experiment procedure consisted of the following steps. Firstly, the fibers were aligned under the microscope with the help of a red laser pen. Then the c-band laser was used to maximise the measured signal on the PD by stage aligning and polarization control. The stage is then placed in the electrode gap and a final signal optimization is performed. Afterwards, the safety circuit is closed and the voltage can be turned on. For the free space measurement a maximum of $V_{rms} = 20\,kV$ was used to minimize partial discharges occurring in the electrode gap. For the presented measurement the full voltage range of $V_{rms} = 20\,kV$ was used for the sinusoidal signal with frequency $f = 50$ Hz. The laser wavelength was set to $\lambda_2 = 1549.91$ nm.

B. RESULTS

In a first step, the optical spectra after removing the electrodes were checked in the setup of this section. For this a coarse wavelength sweep was performed that confirmed the initially measured spectra around λ_2. The measured spectra agree well, but are not plotted again. The measurement of the modulated signal is shown in Fig. 15. A linear slope of $\sim (10\,mV)/(1\,kV/cm)$ can be approximated. Towards both
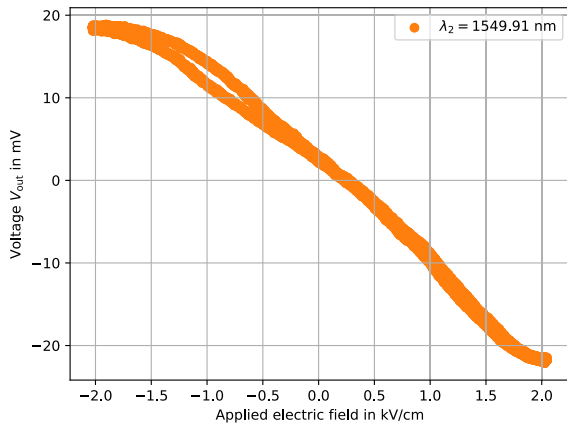
FIGURE 15. Voltage measured with the setup in Fig. 13 and plotted as a function of the applied electrical field (ac, 50 Hz) for a wavelength of $\lambda = 1549.91$ nm. Signal averaged over 128 cycles.

extremes the curve starts to flatten above/below ± 1.5 kV/cm. Only a small and asymmetric hysteresis is visible.

C. DISCUSSION

The comparison of the measurement with electrode (Fig. 12) and in free space (Fig. 15) shows that the general shape of the curve is the same. However, the hysteresis effect and the noise level is much smaller for the free space setup. The applied nominal electric field range was ~ 5 times larger for the electrodes and further studies are required to see how the chip performs in free space for larger fields.

VI. CONCLUSION AND OUTLOOK

The suitability of lithium niobate for e-field sensing was shown by successfully testing a commercial MZM at low frequencies. Afterwards, the results with the MZM on the LNOI platform were confirmed, validating the fabrication process as well as the experiment setup to test those chips.

The RR characteristics were used as a field sensor on chip with a local electric field. The comparison to free space showed the same or even better behavior, leading to the conclusion that results and characteristics of the chip with electrodes can be adopted directly to the free space setting. This allows for fast and easy testing of future sensors on chip realizations with electrodes. The bigger SNR in free-space is advantageous for sensor applications, but the underlying sensors should be understood.

Limitations, as the partial discharge in the electrode gap, could be overcome by having a different optical connection, specifically replacing the 3D stages with a sensor that is glued to the fiber. A more "packaged" sensor would also allow for tests in a transverse electromagnetic cell to fully characterise the sensor for different frequencies.

The presented work is understood as a "proof-of-concept". The low SNR of the first presented device cannot compete with today's classical high voltage measurement equipment. For future tests, different ring geometries or other resonant structures (for example Bragg gratings) will be studied to investigate their sensitivity and SNR, i.e. their overall

suitability to be used as HV electric field sensors. Optimizing the best found structure is a final step before judging the applicability for laboratory and power grid measurements.

REFERENCES

[1] A. Küchler, "High voltage measurement techniques," in *High Voltage Engineering: Fundamentals—Technology—Applications* 1st ed. Berlin, Germany: Springer, 2018, pp. 401–426.

[2] P. Bleuler, Y. Xiao, T. Polonelli, B. Stadler, L. Gallina, H. Kirchner, M. Magno and C. M. Franck, "A unified sensor platform for investigating corona effects on overhead lines," *IEEE Trans. Instrum. Meas.*, to be published.

[3] S. V. Marchese, K. Bohnert, S. Wildermuth, J. L. M. van Mechelen, O. Steiger, L. C. Rodoni, G. Eriksson, and J. Czyzewski, "Optischer Hochspannungssensor mit ol-und gas-freier isolation," in *Proc. Sensoren und Messsysteme, Beiträge der ITG/GMA-Fachtagung*, 2014.

[4] A. Kumada, M. Chiba, and K. Hidaka, "Potential distribution measurement of surface discharge by pockels sensing technique," *J. Appl. Phys.*, vol. 84, no. 6, pp. 3059–3065, Sep. 1998.

[5] N. A. F. Jaeger and F. Rahmatian, "Integrated optics pockels cell high-voltage sensor," *IEEE Trans. Power Del.*, vol. 10, no. 1, pp. 127–134, 1995, doi: 10.1109/61.368406.

[6] E. L. Wooten, K. M. Kissa, A. Yi-Yan, E. J. Murphy, D. A. Lafaw, P. F. Hallemeier, D. Maack, D. V. Attanasio, D. J. Fritz, G. J. McBrien, and D. E. Bossi, "A review of lithium niobate modulators for fiber-optic communications systems," *IEEE J. Sel. Topics Quantum Electron.*, vol. 6, no. 1, pp. 69–82, Jan. 2000, doi: 10.1109/2944.826874.

[7] A. Maeder, H. Weigand, and R. Grange, "Lithium niobate on insulator from classical to quantum photonic devices," *Photoniques*, vol. 116, pp. 48–53, Nov. 2022, doi: 10.1051/photon/202211648.

[8] F. Kaufmann, G. Finco, A. Maeder, and R. Grange, "Redeposition-free inductively-coupled plasma etching of lithium niobate for integrated photonics," *Nanophotonics*, vol. 12, no. 8, pp. 1601–1611, Apr. 2023, doi: 10.1515/nanoph-2022-0676.

[9] D. Pohl, A. Messner, F. Kaufmann, M. R. Escale, J. Holzer, J. Leuthold, and R. Grange, "100-GBd waveguide Bragg grating modulator in thin-film lithium niobate," *IEEE Photon. Technol. Lett.*, vol. 33, no. 2, pp. 85–88, Jan. 15, 2021, doi: 10.1109/LPT.2020.3044648.

[10] J. P. Sharkey, D. C. W. Foo, A. Kabla, J. J. Baumberg, and R. W. Bowman, "A one-piece 3D printed flexure translation stage for open-source microscopy," *Rev. Sci. Instrum.*, vol. 87, no. 2, Feb. 2016, Art. no. 025104, doi: 10.1063/1.4941068.

[11] Q. Meng, K. Harrington, J. Stirling, and R. Bowman, "The openflexure block stage: Sub-100 nm fibre alignment with a monolithic plastic flexure stage," *Opt. Exp.*, vol. 28, no. 4, pp. 4763–4772, 2020, doi: 10.1364/OE.384207.

[12] E. Puma, R. Cheng, J. Holzgrafe, A. Shams-Ansari, R. Shankar, and M. Loncar, "Mitigating anomalous sub-megahertz frequency response of electro-optic phase modulators in X-cut lithium niobate on insulator," in *Proc. Conf. Lasers Electro-Opt. (CLEO)*, May 2022, pp. 1–2, doi: 10.1364/CLEO_SI.2022.SF2O.1.

[13] Thorlabs. *LN81S-FC—10 GHz Intensity Modulator, X-Cut, FC/PC Connectors, 1525 nm—1605 nm*. Accessed: Apr. 14, 2023. [Online]. Available: https://www.thorlabs.com/thorproduct.cfm?partnumber=LN81S-FC

[14] Keysight Technologies. *81608A Tunable Laser Source, High Power and Low SSE, Value Line*. Accessed: Apr. 14, 2023. [Online]. Available: https://www.keysight.com/us/en/product/81608A/81608a-tunable-laser-source-high-power-low-sse-value-line.html

[15] Thorlabs. *DET08CFC/M—5 GHz InGaAs FC/PC-Coupled Photodetector, 800–1700 nm, M4 Tap*. Accessed: Apr. 14, 2023. [Online]. Available: https://www.thorlabs.com/thorproduct.cfm?partnumber=DET08CFC/M

[16] OMICRON Lab. *Vector Network Analyzer—Bode 100*. Accessed: Apr. 14, 2023. [Online]. Available: https://www.omicron-lab.com/products/vector-network-analysis/bode-100

[17] Thurlby Thandar Instruments. *AIM-TTI PL155 Power Supply*. Accessed: Apr. 14, 2023. [Online]. Available: https://www.tme.eu/en/details/pl155-p/programmable-power-supplies/aim-tti

[18] M. R. Escalé, "Generation, modulation and detection of light in lithium niobate nanophotonic devices," Ph.D. dissertation, Dept. Phys., ETH Zürich, Zürich, Switzerland, 2019.

[19] S. Toroghi and P. Rabiei, "Thin film lithium niobate electric field sensors," *Rev. Sci. Instrum.*, vol. 93, no. 3, Mar. 2022, Art. no. 034702, doi: 10.1063/5.0080504.

[20] Keysight Technologies. *N7779C Step-Tunable Laser Source, High Power and Low SSE, Basic Line*. Accessed: Apr. 14, 2023. [Online]. Available: https://www.keysight.com/ch/de/product/N7779C/step-tunable-laser-source-high-power-low-sse-basic-line.html

[21] Artisan Technology Group. *Newport/New Focus 2011-FC 200-kHz Front-End Photoreceiver*. Accessed: Apr. 14, 2023. [Online]. Available: https://www.artisantg.com/TestMeasurement/49008-1/Newport-New-Focus-2011-FC-200-kHz-Front-End-Photoreceiver#

[22] TiePie Engineering. *WiFiScope WS5 WiFi Oscilloscope*. Accessed: Apr. 14, 2023. [Online]. Available: https://www.tiepie.com/en/wifi-oscilloscope/wifiscope-ws5

[23] Thorlabs. *HVA200—High-Voltage Amplifier, ±200 V*. Accessed: Apr. 14, 2023. [Online]. Available: https://www.thorlabs.com/thorproduct.cfm?partnumber=HVA200

[24] D. E. Zelmon, D. L. Small, and D. Jundt, "Infrared corrected Sellmeier coefficients for congruently grown lithium niobate and 5 mol. % magnesium oxide–doped lithium niobate," *J. Opt. Soc. Amer. B, Opt. Phys.*, vol. 14, no. 12, pp. 3319–3322, 1997, doi: 10.1364/JOSAB.14.003319.

[25] Y. Xu, M. Shen, J. Lu, J. B. Surya, A. Al Sayem, and H. X. Tang, "Mitigating photorefractive effect in thin-film lithium niobate microring resonators," *Opt. Exp.*, vol. 29, no. 4, pp. 5497–5504, 2021, doi: 10.1364/OE.418877.

[26] Thorlabs. *Fiber-Coupled, Benchtop Tunable Laser Sources*. Accessed: Apr. 14, 2023. [Online]. Available: https://www.thorlabs.com/newgrouppage9.cfm?objectgroup_id=9997

[27] Thorlabs. *FPC562—Fiber Polarization Controller, 3 Ø56 mm Paddles, SMF-28e+, FC/APC Connectors*. Accessed: Apr. 14, 2023. [Online]. Available: https://www.thorlabs.com/thorproduct.cfm?partnumber=FPC562

[28] R. Bowman, E. Meng, and J. Stirling. *OpenFlexure Block Stage*. Accessed: Apr. 14, 2023. [Online]. Available: https://openflexure.gitlab.io/openflexure-block-stage/

[29] E. Huber, M. Mirzaee, J. Bjorgaard, M. Hoyack, S. Noghanian, and I. Chang, "Dielectric property measurement of PLA," in *Proc. IEEE Int. Conf. Electro Inf. Technol. (EIT)*, May 2016, pp. 788–792.

ANDREAS MAEDER received the B.Sc. and M.Sc. degrees in physics from the Swiss Federal Institute of Technology (ETH) Zürich, Zürich, Switzerland, in 2017 and 2020, respectively, where he is currently pursuing the Ph.D. degree with the Optical Nanomaterial Group, Department of Physics (D-PHYS).

His current research interests include exploring thermo- and electro-optic effects in lithium niobate-on-insulator to realize reconfigurable integrated circuits for classical and quantum applications.

RACHEL GRANGE received the Diploma degree in physics from the Swiss Federal Institute of Technology Lausanne (EPFL), Lausanne, Switzerland, in 2002, and the Ph.D. degree from the Swiss Federal Institute of Technology (ETH) Zürich, Zürich, Switzerland, in 2006.

From 2007 to 2010, she was a Postdoctoral Researcher with EPFL, involved in nonlinear bioimaging with metal-oxides nanoparticles. From 2011 to 2014, she was the Junior Group Leader with Friedrich Schiller University Jena, Germany. She is currently an Associate Professor of integrated optics and nanophotonics with the Department of Physics, ETH Zürich. Her current research interest includes metasurfaces, complex materials, and on-chip lithium niobate devices.

DANIEL WACKERNAGEL received the B.Sc. and M.Sc. degrees in electrical engineering and information technology from the Swiss Federal Institute of Technology (ETH) Zürich, Switzerland, in 2016 and 2018, respectively, where he is currently pursuing the Ph.D. degree with the High Voltage Laboratory, Department of Information Technology and Electrical Engineering (D-ITET).

His current research interest includes electro-optical measurements in high voltage environments.

FABIAN KAUFMANN received the B.Sc. and M.Sc. degrees in physics from the Swiss Federal Institute of Technology (ETH) Zürich, Zürich, Switzerland, in 2014 and 2017, respectively, where he is currently pursuing the Ph.D. degree with the Optical Nanomaterial Group, Department of Physics (D-PHYS).

His current research interest includes fabrication and light coupling for lithium niobate on insulator integrated photonic chips for classical and quantum applications.

CHRISTIAN M. FRANCK (Senior Member, IEEE) received the Diploma degree in physics from the University of Kiel, Kiel, Germany, in 1999, and the Ph.D. degree in physics from the University of Greifswald, Greifswald, Germany, in 2003.

From 2003 to 2009, he was with the ABB Swiss Corporate Research Center, Switzerland, as a Scientist and the Group Leader for gas circuit breakers and high voltage systems. He is currently a Full Professor of high voltage technology with the Swiss Federal Institute of Technology (ETH) Zürich, Zürich, Switzerland. His current research interests include gaseous and solid insulation systems and switching arcs.

● ● ●